JOURNAL OF GEOPHYSICAL RESEARCH, VOL. 105, NO. B5, PAGES 10,791–10,806, MAY 10, 2000

Synthetic aperture radar interferometry of Okmok volcano, Alaska: Radar observations

Zhong Lu
Raytheon STX Corporation, EROS Data Center, U.S. Geological Survey, Sioux Falls, South Dakota

Dörte Mann and Jeffrey T. Freymueller
Geophysical Institute, University of Alaska, Fairbanks

David J. Meyer
Raytheon STX Corporation, EROS Data Center, U.S. Geological Survey, Sioux Falls, South Dakota

Abstract. ERS-1/ERS-2 synthetic aperture radar interferometry was used to study the 1997 eruption of Okmok volcano in Alaska. First, we derived an accurate digital elevation model (DEM) using a tandem ERS-1/ERS-2 image pair and the preexisting DEM. Second, by studying changes in interferometric coherence we found that the newly erupted lava lost radar coherence for 5-17 months after the eruption. This suggests changes in the surface backscattering characteristics and was probably related to cooling and compaction processes. Third, the atmospheric delay anomalies in the deformation interferograms were quantitatively assessed. Atmospheric delay anomalies in some of the interferograms were significant and consistently smaller than one to two fringes in magnitude. For this reason, repeat observations are important to confidently interpret small geophysical signals related to volcanic activities. Finally, using two-pass differential interferometry, we analyzed the preeruptive inflation, coeruptive deflation, and posteruptive inflation and confirmed the observations using independent image pairs. We observed more than 140 cm of subsidence associated with the 1997 eruption. This subsidence occurred between 16 months before the eruption and 5 months after the eruption, was preceded by ~18 cm of uplift between 1992 and 1995 centered in the same location, and was followed by ~10 cm of uplift between September 1997 and 1998. The best fitting model suggests the magma reservoir resided at 2.7 km depth beneath the center of the caldera, which was ~5 km from the eruptive vent. We estimated the volume of the erupted material to be 0.055 km^3 and the average thickness of the erupted lava to be ~7.4 m.

1. Introduction

Repeat-pass synthetic aperture radar (SAR) interferometry has become an important technique to measure volcanic deformation at a horizontal resolution of tens of meters with a vertical accuracy of centimeters to subcentimeters. *Massonnet et al.* [1995] applied SAR interferometry at the Mt. Etna volcano and detected ~14 cm of deflation associated with the 1993 eruption. Deformation measured with repeat-pass SAR interferometry has been reported for numerous volcanoes worldwide [*Rosen et al.*, 1996; *Briole et al.*, 1997; *Lu et al.*, 1997, 1998; *Sigmundsson et al.*, 1997, 1999; *Thatcher and Massonnet*, 1997; *Fujiwara et al.*, 1998; *Lanari et al.*, 1998; *Wicks et al.*, 1998; *Jonsson, et al.*, 1999].

In this paper, we document significant volcanic deformation of the Okmok volcano before, during, and after the 1997 eruption using ERS-1 and ERS-2 SAR images acquired in 1992, 1993, 1995, 1997, and 1998. Deformation observations were verified using independent interferograms that span the same time intervals but with different acquisition times. These independent observations are important for assessing the errors in the interferograms. We carefully analyzed error sources that can affect the interferograms, including errors in the digital elevation model (DEM) and atmospheric errors. We analyzed the interferometric coherence within the caldera to study the temporal changes in coherence of the 1997 lava flow. Preliminary results of SAR interferometric measurement of deformation associated with the February-April 1997 Okmok eruption were reported by *Lu et al.* [1998]. The interferograms shown here cover larger regions than those presented by *Lu et al.* [1998]. A forthcoming paper will include more detailed models to explain the deformation observed in these interferograms.

Paper number 2000JB900034.
0148-0227/00/2000JB900034$09.00

1.1. Okmok Volcano

Okmok volcano, a broad shield topped with a 10-km-wide caldera, occupies most of the northeastern end of Umnak Island, Alaska (Figures 1a and 1b). Catastrophic pyroclastic caldera-forming eruptions occurred ~8000 and 2400 years ago

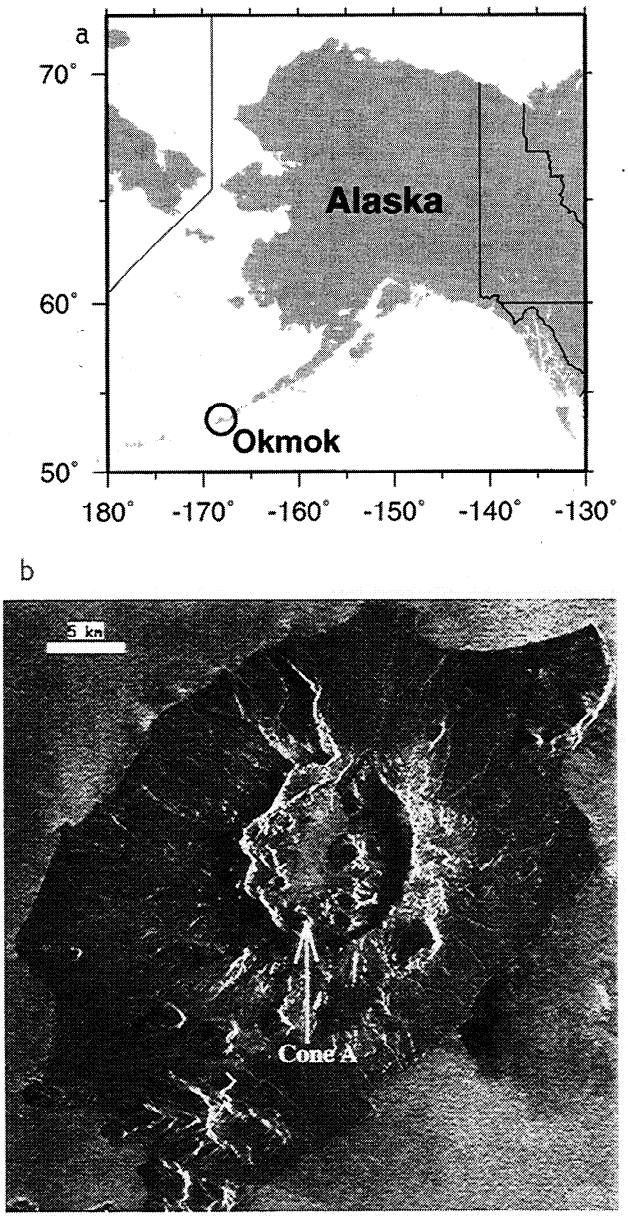

Figure 1. (a) Location of Okmok volcano, Umnak Island, in the central Aleutians, Alaska. (b) ERS-2 synthetic aperture radar amplitude image of Okmok volcano. The image covers the northeastern part of Unmak Island, which is ~40 by 40 km in dimension.

[*Byers*, 1959; *Miller et al.*, 1998]. Several major eruptions and a number of minor events occurred in the caldera in historical time. The sketchy historical record dates back to 1817. Eruptions in this century happened in 1931, 1936, 1938, 1943, 1945, 1958, 1960, 1981, 1983, 1986, 1988, and 1997 [*Byers*, 1959; *Miller et al.*, 1998]. All historical eruptions of Okmok originated from Cone A, located on the southern caldera rim, and produced abundant ash emissions and mafic lava flows on the caldera floor (Figure 1b).

The latest eruption of Okmok volcano began on February 11, 1997, when a steam and ash plume was reported. The eruption was a moderate Strombolian type with an ash plume reaching to 9144 m and a lava flow covering an area of ~7.5 km^2 [*Mann et al.*, 1998; *Worley et al.*, 1998]. Satellite thermal imagery and inspection from the air showed that eruptive activity had ceased by late April 1997 [*Dean et al.*, 1998].

Okmok is an ideal target for SAR interferometry because much of the volcano is at a fairly low elevation and the caldera floor has subdued topographic relief. The elevation of the rim of the caldera is ~1070 m. The caldera floor is relatively flat, with <370 m relief. The low elevation implies a longer season without snow cover, extending the interval during which we can expect to obtain coherent data (section 1.2). The low relief minimizes problems of foreshortening, layover, and shadowing and ensures that observations are fairly insensitive to errors in topography.

1.2. SAR Interferometry

Crustal deformation is measured by generating an interferogram using a pair of repeat-pass SAR images. The phase of each pixel in a SAR image corresponds to the distance (path length) from the satellite to each resolution element of the ground surface. An interferogram is an image constructed using the phase difference of images taken on two different satellite passes. Path length changes are related to topography, the difference in the satellite positions between the two passes, ground surface deformation occurring between the image acquisitions, different atmospheric conditions (pressure, temperature, and water vapor content) at the image acquisition times, and noise. In an interferogram the component of the phase change caused by the difference in satellite positions can be removed using satellite position and velocity vectors, and the component contributed by the terrain topography can be removed by using a DEM or another interferogram where deformation is negligible [e.g., *Massonnet and Feigl*, 1998]. This results in an interferogram that contains ground surface deformation, atmospheric delay anomalies, and noise.

An interferogram is usable only in those areas where the radar returns in both images are coherent. Coherent interference of SAR images depends on consistency in the scattering characteristics of the ground surface at the time of radar acquisitions. Reduction of coherence can be caused by factors such as growth of vegetation, changes in land cover type, freezing/thawing of the surface, and random movement of scatterers whose sizes are on the scale of wavelength. Covering the surface with lava or a thick ash layer will completely destroy the interferometric coherence [*Zebker et al.*, 1996]. Therefore, in an interferometric coherence map, regions covered by new lava or significant ash layers have the lowest coherence values because the scattering characteristics in these regions are completely changed. Regions covered with loose materials tend to lose interferometric coherence by some degree due to the movement of the surface materials. *Lu and Freymueller* [1998] carried out a systematic study of interferometric coherence for several types of volcanic surface materials using ERS-1 images acquired over the Katmai volcano group in Alaska. They found that regions dominated by loose surface materials completely lost coherence in C band (wavelength of 5.66 cm) images over a time interval of 1 year but that the measurement of volcanic deformation is possible using C band images acquired during the summer for time separations of up to a few years, as long as the surface is dominated by lava.

Table 1. Interferometric Data Acquisition Parameters

Orbit 1	Orbit 2	Date 1	Date 2	Track	h_a, m	Plate
E1_5878	E1_20250	Aug. 30, 1992	May 30, 1995	222	391	5b
E1_6773	E1_12284	Oct. 31, 1992	Nov. 20, 1993	115	-568	3
E1_12012	E1_22376	Nov. 1, 1993	Oct. 25, 1995	344	-138	2b and 5a
E1_22376	E2_2703	Oct. 25, 1995	Oct. 26, 1995	344	-115	1 and 2a
E1_22147	E2_12494	Oct. 9, 1995	Sept. 9, 1997	115	-695	2c and 6
E1_20372	E2_12723	June 7, 1995	Sept. 25, 1997	344	716	7
E2_12723	E2_17733	Sept. 25, 1997	Sept. 10, 1998	344	108	2e and 8
E2_11721	E2_12723	July 17, 1997	Sept. 10, 1997	344	419	2d and 4a
E2_10719	E2_12723	May 8, 1997	Sept. 10, 1997	344	-130	4c
E2_10719	E2_11721	May 8, 1997	July 17, 1997	344	-99	4b
E2_18005	E2_18506	Sept. 29, 1998	Nov. 3, 1998	115	40	2f

h_a. Altitude of ambiguity.

2. Methods

Because the phase difference of the image pair corresponds to the change in the round-trip path length of radar waves to ground targets, an interferogram is similar to a contour map of the change in distance to the ground surface along the look direction of the satellite. The SAR images used in these studies were collected by the C band (5.66 cm wavelength) ERS-1 and ERS-2 satellites of the European Space Agency (ESA), operated at an altitude of ~790 km. The look direction of the antenna is about 20° to 26° from vertical, and therefore interferograms are more sensitive to vertical deformation than to horizontal. The satellite orbits repeat every 35 days.

For each image pair we optimized the Doppler frequency during SAR image generation. The average Doppler frequency of the two images was used to process the SAR signal data into single-look complex (SLC) images from which the interferograms were produced. This is especially important for interferograms that mix ERS-1 and ERS-2 images, as the two satellites used different Doppler frequencies. Range spectrum filtering for the two SLC images was applied to account for the spectral shift induced by the slight difference in incidence angle between the SLC images [*Gatelli et al.*, 1994], only that common to the two being retained. This optimization procedure improved the interferometric coherence (H. Zebker, personal communication, 1997).

We improved the estimation of the baseline vector, the spatial distance between two orbit trajectories, using the precision orbit data product (PRC) delivered by the German Processing and Archiving Facility (D-PAF) [*Massmann*, 1995]. PRC state vectors are given at 30-s intervals. The accuracy of the PRC position vectors is ~30 cm for along-track and 8 cm for cross-track [*Massmann*, 1995]. In several cases, we further improved the estimate of the interferometric baseline using ground control points [*Rosen et al.*, 1996].

We removed the effect of topography from the interferogram using a DEM and the known satellite orbits, leaving only the contributions of ground deformation, atmospheric delay, and noise. This is the so-called two-pass differential interferometry method [see, e.g., *Massonnet and Rabaute*, 1993]. In general, too few satellite passes were recorded for the three-pass method [see, e.g., *Zebker et al.*, 1994b], which does not require a precise DEM. Before using the two-pass method we derived a DEM from independent SAR data, because the existing U.S. Geological Survey (USGS) [1993] DEM was digitized from a 1:250,000 scale map and was not of sufficient vertical accuracy (see section 3).

Errors in the DEM map directly into apparent surface deformation. The sensitivity to topography is characterized by the altitude of ambiguity, h_a, which is the amount of topographic relief required to generate one interferometric fringe [*Massonnet and Rabaute*, 1993]. Because the altitude of ambiguity is inversely proportional to the component of the baseline projected into the satellite look direction, $B_\perp$, we used interferometric pairs with relatively small baselines for deformation analysis. The associated altitudes of ambiguity range from 40 to 720 m. The phase component contributed by the topography has been removed for all interferograms (Table 1) shown in the following sections unless otherwise noted.

3. Derivation of High-Accuracy DEM With Tandem SAR Interferometry

Interferograms with nonzero baseline contain information contributed by the topography. The errors in the DEM used to produce a deformation interferogram (or topography-removed interferogram) propagate into the deformation measurement. The best preexisting topographic data for the Okmok volcano is the USGS DEM, with 90 m horizontal resolution and a quoted vertical accuracy of 30 m at 90% confidence level [*USGS*, 1993]. Artificial boundaries and spurious elevations are visible in the DEM.

To improve the accuracy of the DEM, we first generated an interferogram using tandem ERS-1/ERS-2 images acquired on October 25 and 26, 1995. So-called tandem pairs were acquired by adjusting the ERS-1 and ERS-2 orbits, which repeat every 35 days, to follow one another by 1 day. Thus a point on the surface was imaged by one satellite (ERS-1) on a given day and by the other satellite (ERS-2) on the following day. The October 1995 pair is the only tandem pair with suitable coherence acquired by the ERS satellites at Okmok volcano because the remaining pairs were collected during the winter. The two images are spaced only 1 day apart, so we can assume that the deformation is negligible.

Errors in knowledge of the interferometric baseline introduce systematic long-wavelength biases that could be

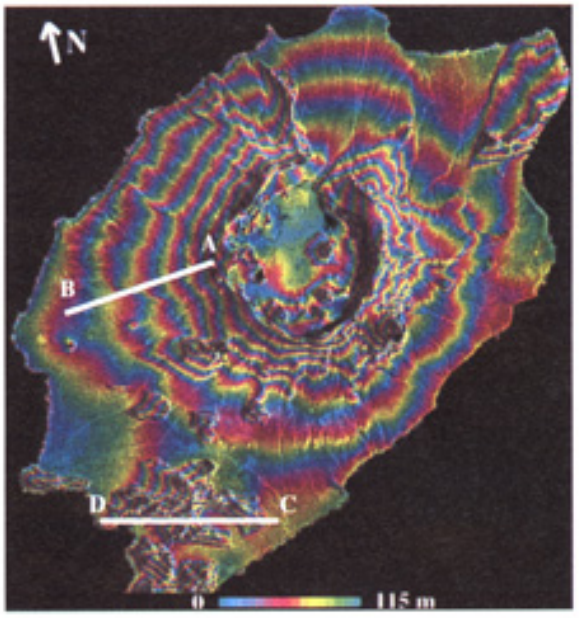

Plate 1. Tandem ERS-1/ERS-2 interferogram of Okmok volcano, which is used to refine the preexisting USGS DEM. One fringe represents 115-m topographic relief.

corrected given enough ground control points (GCP). We tried to remove such possible systematic biases using the technique proposed by *Rosen et al.* [1996], which is to estimate the baseline using the unwrapped interferometric phase and many GCPs extracted from topographic heights (i.e., the existing USGS DEM) available in the same coordinate system as the interferogram. This procedure is also needed because we have to estimate the absolute phase values in the unwrapped interferogram for constructing elevation heights [e.g., *Zebker et al.*, 1994a]. To account for the possible errors in the existing DEM, we used more than 5000 GCPs extracted automatically from the existing USGS DEM. Because of the number of GCPs used, the possible errors in the existing DEM do not bias the estimate of baseline. The restitute vectors are from ESA's PRC, so the refined baseline does not differ very much from the one without GCPs. The baseline $B_\perp$ for the interferogram is 83 m, which corresponds to h_a = 115 m. There is not much vegetation on the volcano surface; therefore it is theoretically possible to generate a DEM with accuracy of ~10 m [*Wu et al.*, 1996].

Plate 1 shows the interferogram used to derive the DEM, with the effect of topography included. Each cycle of colors represents topographic relief of ~115 m. The interferometric correlation coefficient on average is larger than 0.9, which indicates excellent coherence over almost the entire image. Areas with severe SAR geometric distortion effects, such as the west edge of the caldera and mountain peaks, have lower coherence. The interferometry-derived DEM has a variable height accuracy, with lower accuracy in regions of lower coherence. After unwrapping the phase of the interferogram [*Goldstein et al.*, 1988] we produced an interferometry-derived DEM.

Height differences between the interferometry-derived DEM and the USGS DEM, as well as the heights of the USGS DEM along two profiles, are shown in Figures 2a and 2b. For the profile A-B the topographic relief is ~800 m, and the height difference between the two DEMs ranges from −7 m to 37 m (Figure 2a). The discontinued curve for the height difference is caused by that interferometry-derived DEM is not valid for regions with severe SAR geometric distortions or coherence loss. Height differences are not correlated with the terrain height, which indicates that the height difference is not caused by the error in baseline estimation. For profile C-D (13 km long) we found the height differences range from −60 m to 35 m (Figure 2b).

We tested the accuracy of the interferometry-derived DEM using an interferogram made with SAR images acquired in

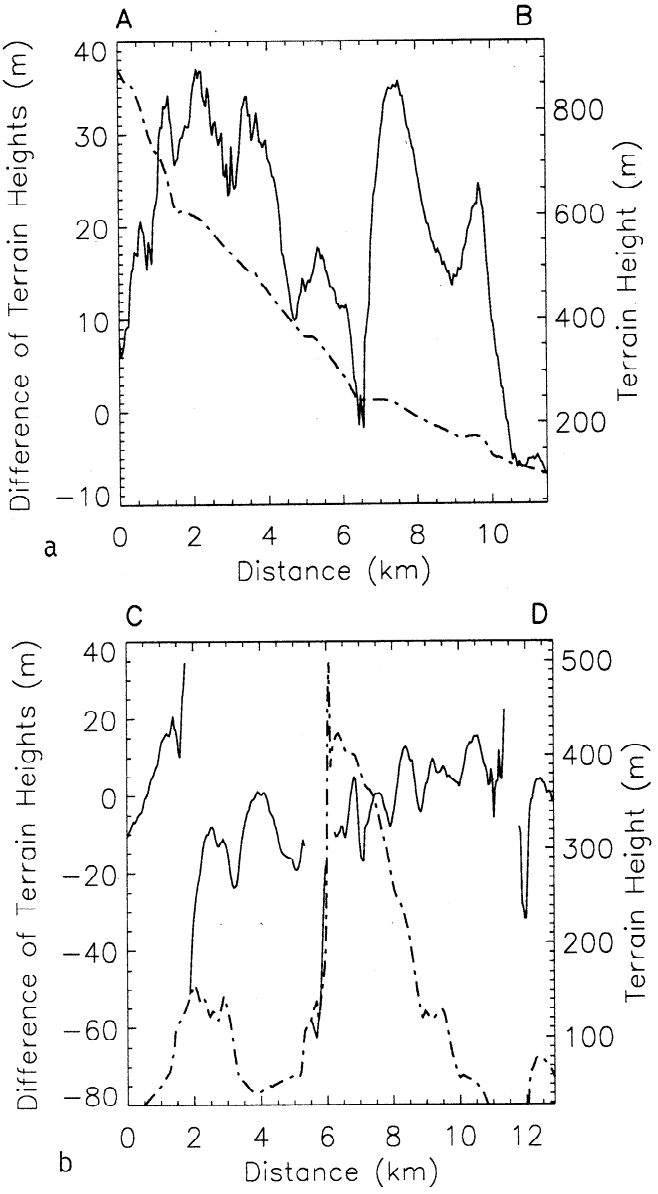

Figure 2. (a) The terrain height of the USGS DEM (dashed line) and height difference between interferometry-derived DEM and the USGS DEM (solid line) along the profile A-B. The positions of A and B are shown in Plate 1. (b) The terrain height of the USGS DEM (dashed line) and height difference between interferometry-derived DEM and the USGS DEM (solid line) along the profile C-D . The positions of C and D are shown in Plate 1.

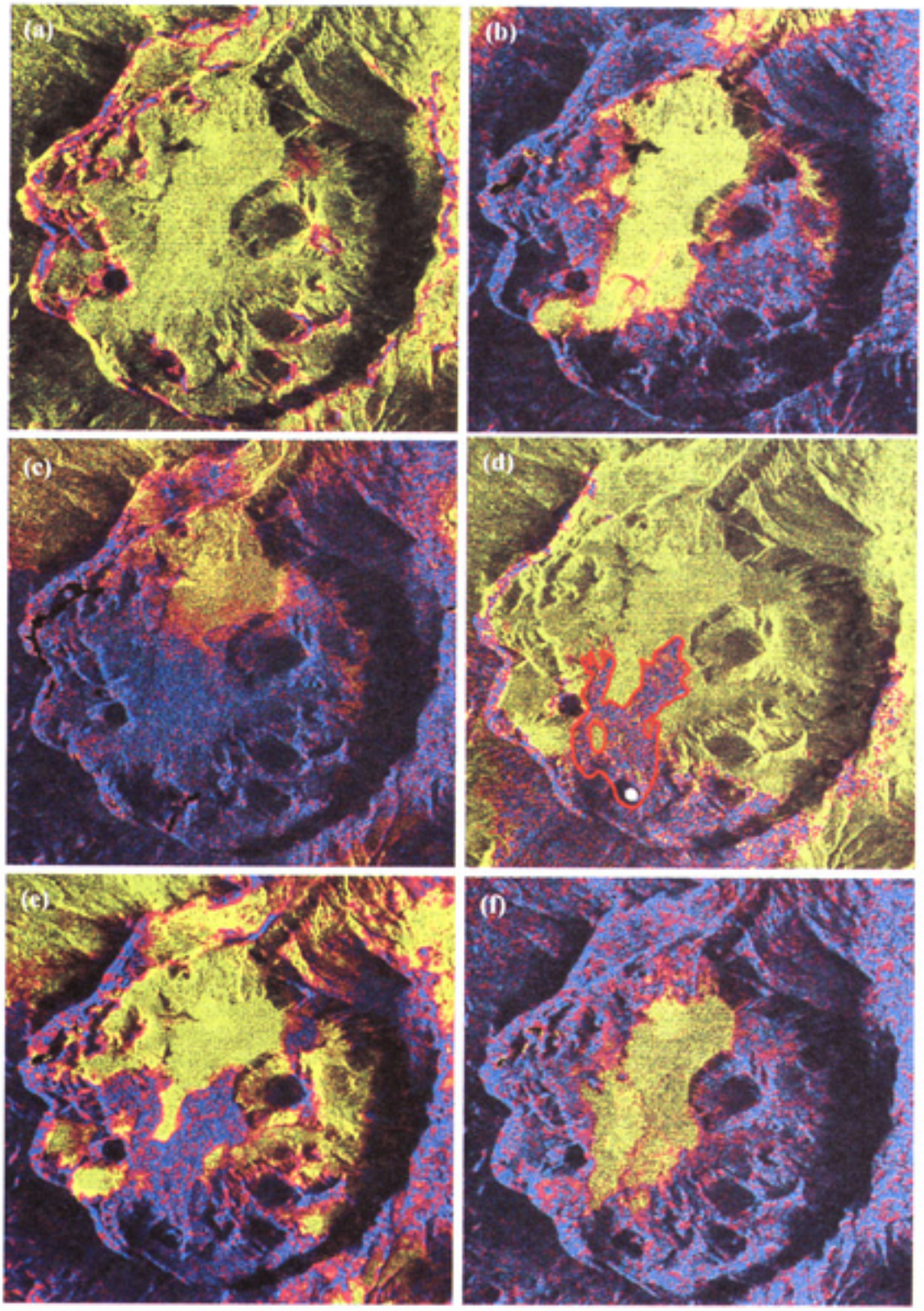

Plate 2. Interferometric coherence within the Okmok caldera constructed using pairs of images acquired on (a) October 25 and 26 1995 (1-day separation); (b) November 1, 1993 and October 25, 1995 (2-year separation); (c) October 9, 1995 and September 9, 1997 (2-year separation); (d) July 17 and September 25, 1997 (2-month separation); (e) September 25, 1997, and September 10, 1998 (1-year separation); (f) September 29 and November 2, 1998, one and a half years after the eruption. Yellow regions indicate high coherence, while purple and red regions indicate lower coherence. Approximate outline of 1997 lava flow is outlined in red (Plate 2d). The white dot in Plate 2d represents the eruption center.

October and November 1995 (35 days time separation). The baseline $B_\perp$ for the interferogram is about 399 m, and ha is ~23 m, so it is very sensitive to topography: about 23 m uncorrected topographic relief will produce a fringe in the interferogram. We compared topography-removed interferograms derived using the USGS DEM and the interferometry-derived DEM. We found there were more residual fringes in the topography-removed interferogram done with the USGS DEM than in the one with the interferometry-derived DEM. The residual fringes are most likely caused by the errors in the DEMs because (1) they occur in high relief regions and follow the topographic contours; (2) they do not resemble the deformation we observe in other interferograms; and (3) the residual fringes are much greater in magnitude than any atmospheric errors seen in other images. Therefore we conclude that the interferometry-derived DEM is more accurate than the preexisting USGS DEM. Accuracy of the interferometry-derived DEM is better than 15 m in areas of good coherence.

We could not compute valid heights for regions with low interferometric coherence and regions with severe layover and foreshortening effects. This left several "holes" in the interferometry-derived DEM. To fill in these holes, we merged the two DEMs, resampling the USGS DEM to 20-m horizontal spacing where data were missing in the interferometry-derived DEM. Our conservative estimate is that the final DEM has a vertical accuracy of ~30 m, although it is most likely much better than that in most of the region

4. Temporal Changes of Interferometric Coherence

An interferometric coherence map shows the spatial variation in the interferometric correlation coefficient [e.g., *Lu and Freymueller*, 1998; *Zebker and Villasenor*, 1992; *Zebker et al.*, 1996]. It measures changes of both phase and intensity of backscattering signals and is sensitive to the movement of scatterers within each resolution element. In Plate 2, we show the interferometric coherence maps for six time intervals, both before and after the eruption. Yellow regions indicate high coherence, while purple and red regions indicate lower coherence. For simplicity, we limited our study to the changes of interferometric coherence on the caldera floor. On the basis of SAR amplitude images, it is difficult to distinguish regions covered with pre-1997 lava from those covered with 1997 lava. However, backscattering characteristics of SAR signals for regions with new lava changed with time; the interferometric coherence map can be used to detect such changes and therefore separate the new lava from pre-1997 lava.

Plate 2a shows a coherence map generated from a tandem ERS-1/ERS-2 image pair. Regions with high coherence in Plate 2b (1993-1995) correspond mostly to pre-1997 lava flows; areas covered with looser surface materials have lost coherence in the 2-year interval between image acquisitions. This is consistent with other SAR coherence results from the Katmai volcano group in *Alaska [Lu and Freymueller*, 1998]. Plate 2c (1995-1997) indicates that only the northern part of the pre-1997 lava flow maintained good coherence. This is because the southern part of the pre-1997 lava flow was covered with both new lava and ash from the 1997 eruption.

The most interesting feature is shown in Plate 2d (July–September 1997), which was generated from images acquired 3 and 5 months after the eruption. The lower coherence within the caldera floor corresponds mostly to regions covered by 1997 lava. Even though the eruption ended 3 months before the first image was acquired, areas covered with new lava remain completely incoherent. A reconnaissance field survey in the summer of 1998 confirmed that the two-pronged 1997 lava flow on the caldera floor matches the incoherent region of this interferogram [*Mann et al.*, 1998]. The incoherent region to the east of Cone A is probably due to snow cover in one or both of the images, since that region is located at a higher elevation and was covered with snow in August 1998. Low coherence also is found for the area covered with 1997 lava flows in Plate 2e (September 1997 to September 1998). However, an image pair covering the time interval September to November 1998 (Plate 2f) shows high coherence for this region.

We propose that the lack of coherence for the new lava flow in the months after the eruption and the recovery of coherence after 5-17 months strongly suggest that the settling and compaction caused by cooling and the weathering of the new lava flow control the coherence in the months to years immediately after an eruption. The 1997 lava flow is a blocky flow similar to Hawaiian a'a lava and locally was ~8 m thick. During cooling, individual blocks may shift or settle. Since many of the blocks are the optimum size to act as backscatterers, shifting of the blocks relative to one another would significantly modify the radar return signal and destroy phase coherence. However, simple global compaction (or shrinkage) of the whole pile of lava by cooling would probably not change the surface layer, which would then presumably result in an observable signal. Weathering of the fragile new lava would also reduce the radar coherence. Our observations suggest that these processes continued for at least 5 months, but <17 months, after the eruption.

5. Atmospheric Delay Anomalies

ERS-1 and ERS-2 sensors orbit at an altitude of ~790 km. The electromagnetic wave from these sensors must propagate through the ionosphere, the stratosphere, and the troposphere. Therefore the radar pulses are subject to small variations in the index of refraction along the line of propagation. Differences in the temperature, pressure, and water vapor content of the atmosphere between the two observation times cause changes in the atmospheric path delay that introduce errors in the observed interferogram [*Massonnet and Feigl*, 1995; *Tarayre and Massonnet*, 1996]. *Zebker et al.* [1997] indicated that variations of atmospheric water vapor contributed most of the atmospheric anomaly delays. Spatial and temporal changes of 20% in relative humidity could lead to 10-cm errors in repeat-pass interferometric deformation maps.

We analyzed the atmospheric effects on the deformation map shown in Plate 3. Atmospheric delay anomalies outside of the caldera are severe. The altitude of ambiguity for the interferogram is ~570 m; an error of 570 m in the DEM would produce just one fringe. Therefore the fringes along profiles C-D and E-F in the southern and southwestern parts of the island cannot be due to errors in the DEM. Since they are not likely to be caused by deformation, these fringes are most likely caused by atmospheric delays. Figure 3a shows the range changes and topography along profile C-D. The range change caused by atmospheric anomaly is ~3 cm over a

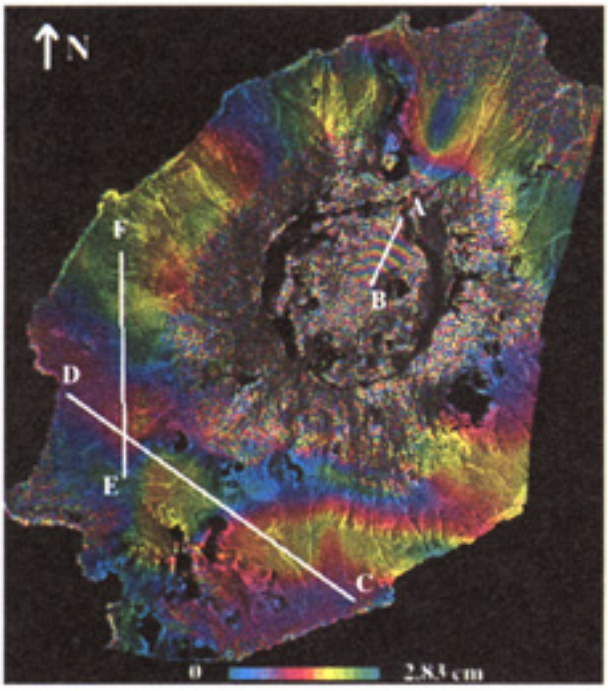

Plate 3. Topography-removed interferogram spanning 1992 to 1993. Volcanic deformation along the profile A-B is shown in Figure 5a.

distance of 18 km. Figure 3b shows the range change along profile E-F, where a range change of ~2 cm was observed over a distance of 12 km.

Plate 4a shows part of a topography-removed interferogram constructed using a pair of images acquired in July and September 1997, 3 and 5 months after the eruption. Range changes along profiles A-B and C-D are shown in Figures 4a and 4b, where up to 6 cm range change was observed. To prove the range changes in Plate 4a were caused by a difference in atmospheric conditions rather than by seismic or volcanic activities, we generated another two interferograms for the same area: one was produced using an image acquired in May 1997 and the July 1997 image (Plate 4b); the other was produced using the May and September 1997 images (Plate 4c). In Plate 4b, we observed fringes similar to the one in the May-July interferogram (Plate 4a). Because the change of colors in Plate 4a is opposite to that in Plate 4b, and because we did not observe any fringe in the May-September interferogram (Plate 4c), we concluded that the fringes in Plates 4a and 4b were caused by an atmospheric anomaly affecting the July 1997 image.

The phase difference caused by the atmospheric delays is significant for interferograms over the Okmok volcano. Range change up to 6 cm was detected over a distance of 8 km (Figure 4b). If the range change is due to change of water vapor content of the atmosphere, ~12% humidity change would lead to such an amount of error [*Zebker et al.*, 1997]. Therefore multiple observations from independent interferograms for similar time intervals should be used to verify any apparent *deformation [Massonnet and Feigl*, 1995]. Nevertheless, atmospheric delay anomalies can dramatically reduce the accuracy of interferometric crustal deformation measurement from subcentimeter in ideal conditions to 2~3 cm.

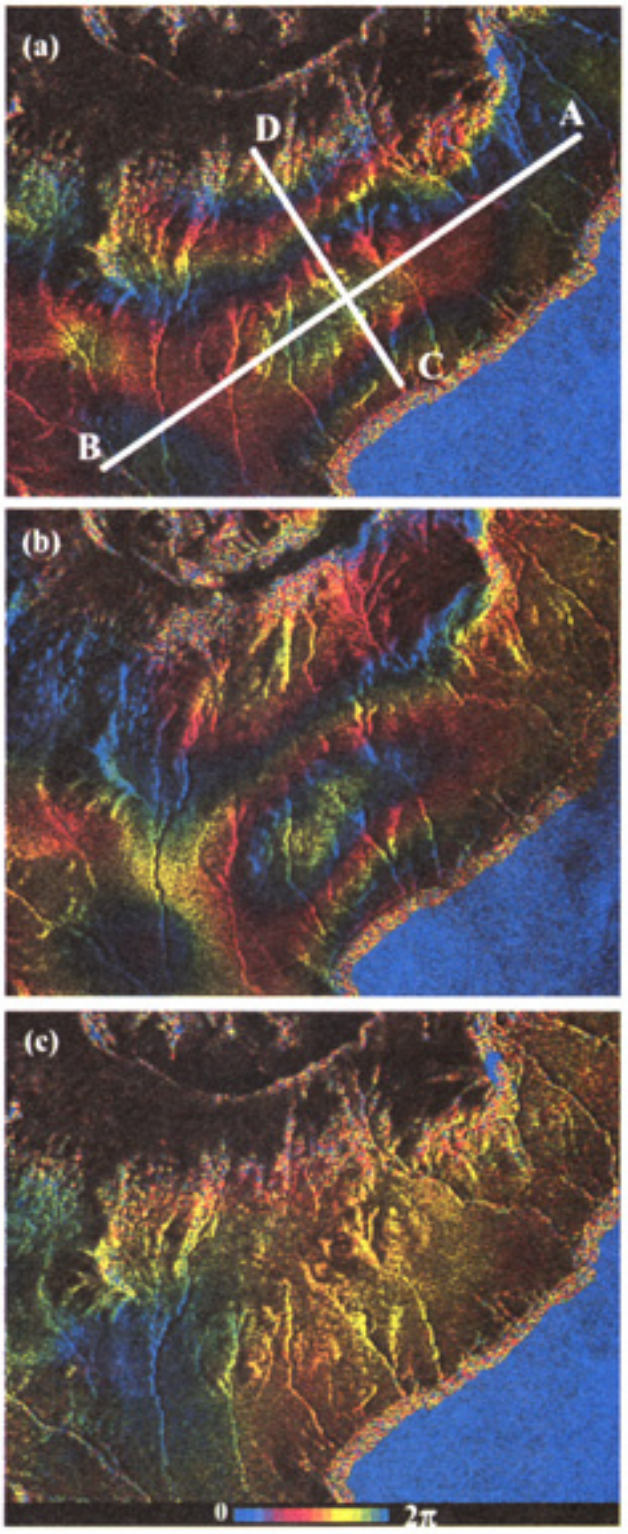

Plate 4. (a) A portion of a topography-removed interferogram with severe atmospheric anomalies. Images used to produce the interferogram were acquired in July and September 1997. Range changes due to the atmospheric delay anomalies along profiles A-B and C-D are shown in Figures 4a and 4b, respectively. (b) A portion of a topography-removed interferogram with severe atmospheric anomalies. Images used to produce the interferogram were acquired in May and July 1997. (c) A portion of a topography-removed interferogram with severe atmospheric anomalies. Images used to produce the interferogram were acquired in May and September 1997.

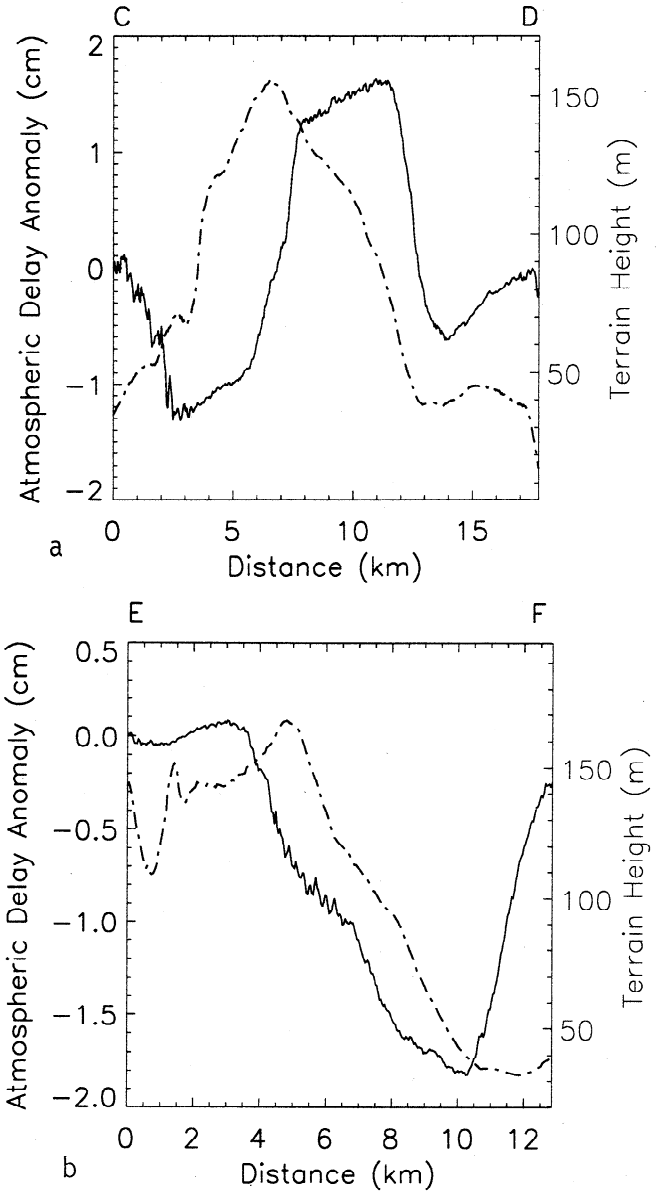

Figure 3. (a) Range change due to the atmospheric delay anomalies (solid line) and terrain height (dashed line) along the profile C-D. The positions of C and D are shown in Plate 3. (b) Range change due to the atmospheric delay anomalies (solid line) and terrain height (dashed line) along the profile E-F. The positions of E and F are shown in Plate 3.

6. Observed Deformation

6.1. Preeruptive Inflation: 1992-1995

We generated a topography-removed interferogram for the time period spanning October 31, 1992, to November 20, 1993 (Plate 3), to measure ground surface deformation that may have preceded the eruption. We observed more than four fringes corresponding to at least 12 cm uplift of the center of the caldera along profile A-B (Figure 5a). Each fringe caused by ground deformation corresponds to a 2.83 cm change in the distance from satellite to ground between two radar acquisitions. Numerous atmospheric delay anomalies are found on the flanks of the volcano, but they are all less than about one fringe in magnitude.

A topography-removed interferogram generated from images acquired on November 1, 1993, and October 25, 1995 is shown in Plate 5a. The deformation along profile A-B is shown in Figure 5b. A range change of ~7 cm, corresponding to uplift of the center of the caldera, was observed along the 7-km profile (Figure 5b). Range change of a similar magnitude was observed along profile B-C over a distance of 1.8 km (Figure 5c). This interferogram shows evidence for nonaxisymmetric deformation, which could be induced by a complex magma source. Since this second uplift center lies approximately between the center of the caldera and Cone A, it might represent magma traveling from the main magma body toward the eruptive center. Interferometric coherence is reasonably high for the regions outside of the caldera, and atmospheric delay anomalies are apparently small.

The deformation observed in Plates 3 and 5a was derived from four SAR images (Table 1) acquired on descending passes, on which the satellite moved from north to south and looked to the west. We verified the observations using two images (Table 1) acquired on August 30, 1992, and May 30, 1995, when the satellite was in ascending mode, moving from south to north and looking to the east. This deformation interferogram is shown in Plate 5b, and the deformation along

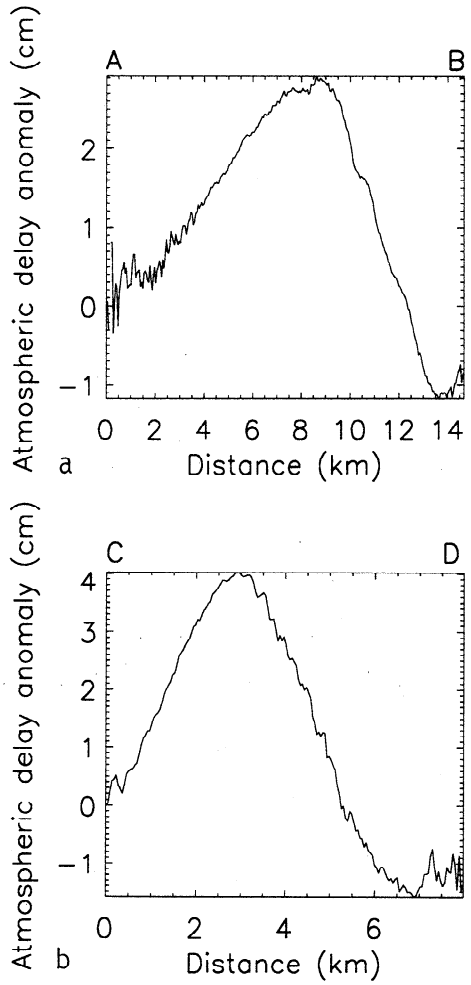

Figure 4. (a) Deformation along profile A-B for the interferogram shown in Plate 4a. The positions of A and B are shown in Plate 4a. (b) Deformation along profile C-D for the interferogram shown in Plate 4a. The positions of C and D are shown in Plate 4a.

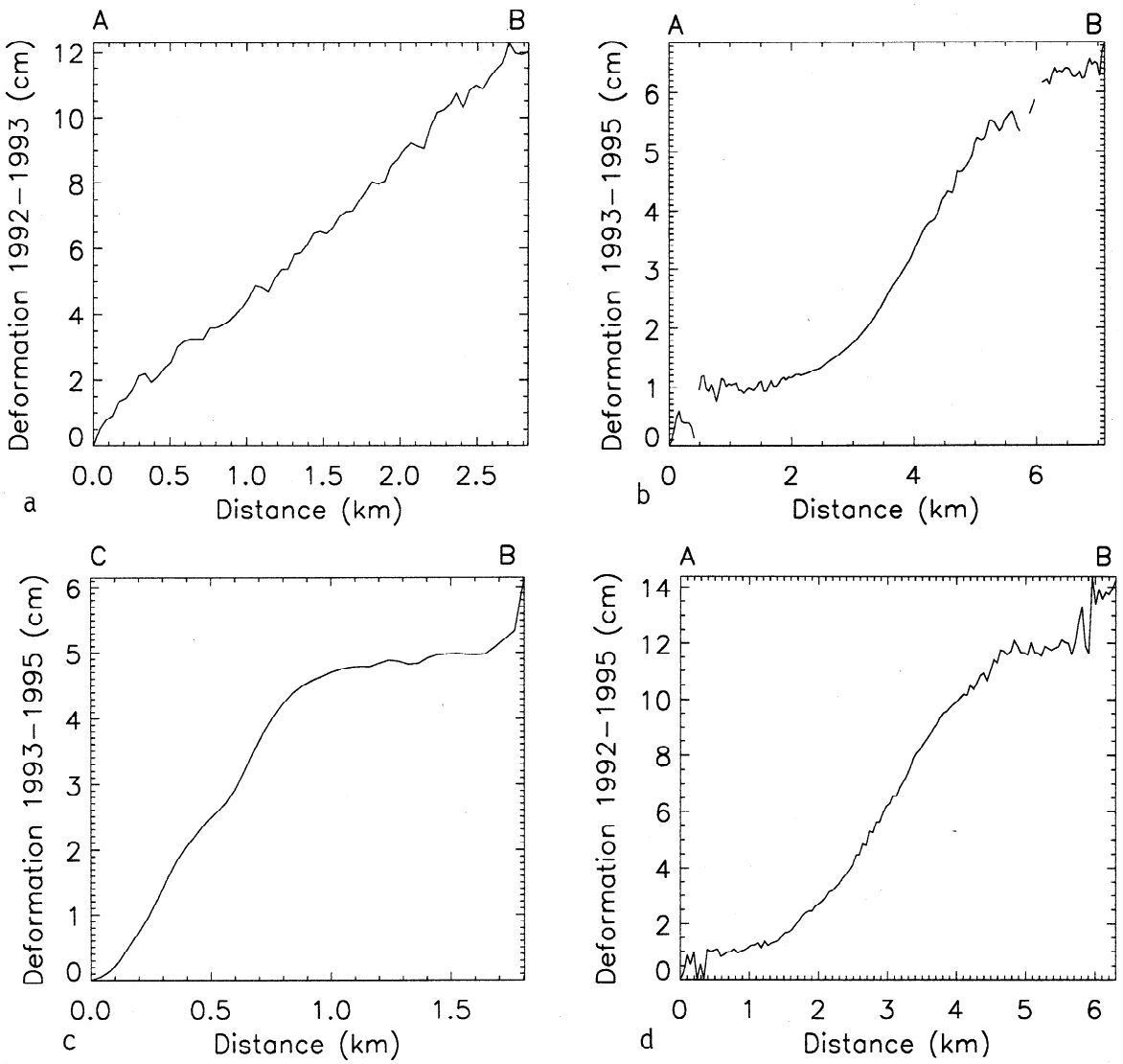

Figure 5. (a) Deformation from 1992 to 1993 along profile A-B. The positions of A and B are shown in Plate 3. (b) Deformation from 1993 to 1995 along profile A-B. The positions of A and B are shown in Plate 5a. (c) Deformation from 1993 to1995 along profile C-B. The positions of C and B are shown in Plate 5a. (d) Deformation from 1992 to 1995 along the profile A-B. The positions of A and B are shown in Plate 5b.

a profile A-B is shown in Figure 5d. The atmospheric delay anomalies are small, and the total deformation is approximately similar to that inferred from the sum of the other two interferograms.

6.2. Coeruptive Deflation (1995-1997)

Plate 6 displays a georeferenced interferogram with topography removed, showing ground deformation between October 9, 1995, and September 9, 1997. More than 50 fringes are visible in the interferogram, so systematic biases, such as topographic errors and atmospheric delays, could account for no more than a small percentage of the observed phase change. The fringes form a clear concentric pattern, centered approximately on the center of the caldera.

Phase coherence is good within and outside the northern half of the caldera and west and southeast of the caldera. The incoherent area within the caldera corresponds mostly to regions covered by loose materials or by new lava from the 1997 eruption. The order of colors (repetitions of blue–yellow–magenta from the caldera outward) indicates that the deformation field is consistent with a deflation source located in roughly the center of the caldera.

We further confirmed the deformation measured in Plate 6 using another independent interferogram spanning approximately the same time interval. Plate 7 shows a topography-removed interferogram constructed using an image pair acquired on June 7, 1995, and September 25, 1997. The two SAR images used to generate Plate 7 are on different tracks from the two used for Plate 6. The satellite look angles for the SAR images used in Plates 6 and 7 are 20.3° and 23.6°, respectively. The interferogram in Plate 7 is independent of the one shown in Plate 6 but shows similar deformation patterns. The interferometric coherence is lower in Plate 7 than in Plate 6, because one of the images used for Plate 7 was acquired on June 7, 1995, when snow may not have completely melted.

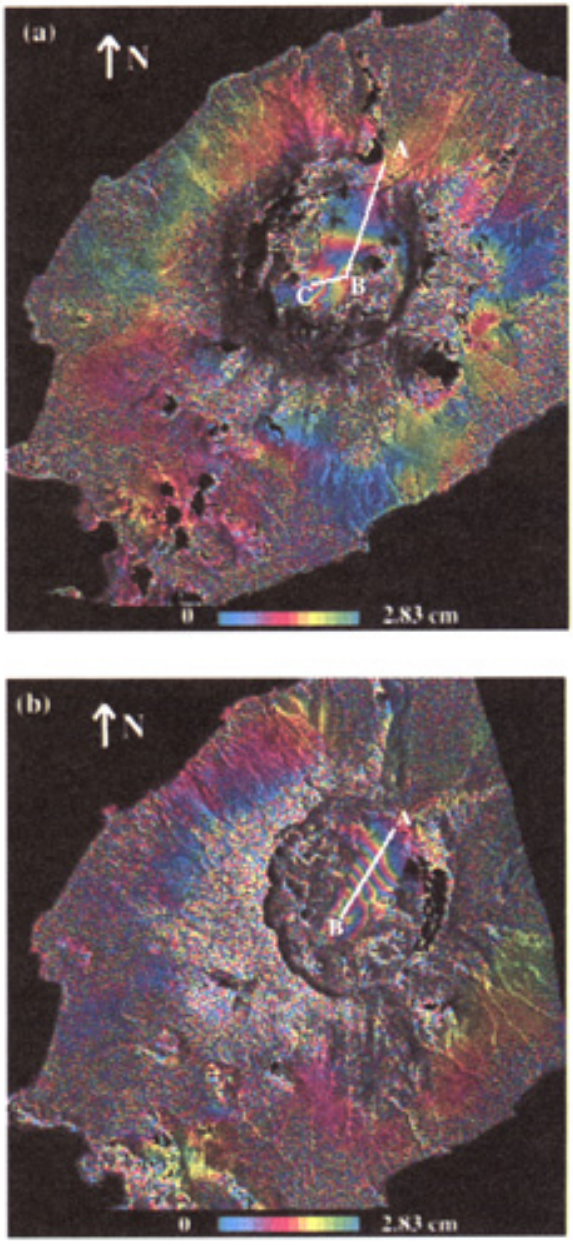

Plate 5. (a) Deformation interferogram spanning 1993 to 1995. Deformation profiles along A-B and C-D are shown in Figures 5b and 5c, respectively. Each fringe represents a 2.83-cm deformation along the satellite look direction. (b) Deformation interferogram spanning 1992 to 1995. Each fringe represents a 2.83-cm deformation along the satellite look direction. Deformation along profile A-B is shown in Figure 5d.

6.3. Posteruptive Inflation (1997-1998)

To study the posteruptive ground surface deformation, we generated a topography-removed interferogram spanning the time interval from September 25, 1997, to September 10, 1998 (Plate 8). Approximately three fringes were observed during the 12-month interval (Figure 6a), indicating that the center of the caldera was uplifted by ~10 cm. The incoherent areas of the interferogram correspond mostly to the regions covered by new lava erupted during February-April 1997 (section 4).

A deformation profile across the 1997 and pre-1997 lava boundaries from C to D (Figure 6b) shows apparent subsidence adjacent to the lobes of the new, incoherent lava flow. The regions to the east of C and regions to the west of D are covered with lava from the February-April 1997 eruption, according to the interferometric coherence map (Plate 2e), which was confirmed by field observations [*Mann et al.*, 1998]. Deformation shown in Figure 6b is relative to a center point of the profile. Figure 6b shows how the pre-1997 lava was deformed locally in response to the 1997 lava flows. During the 12-month period, the regions adjacent to the 1997 flows subsided ~2.0 cm relative to the center of the profile. Loading caused by the 1997 lava might be responsible for this small deformation. Elastic flexure and viscoelastic flexure seem to be unlikely mechanisms. To explain the ~2 cm subsidence caused by the load of an 8-m-thick lava flow would require an elastic thickness on the order of 100 m for the elastic case, which seems exceptionally thin. However, compaction of the pre-1997 flows might be a plausible mechanism for this subsidence. *Briole et al.* [1997] observed similar subsidence near newly erupted lava for the Etna volcano after the 1989 eruption. The deformation was correlated with the area covered by the lava of 1986-87 and

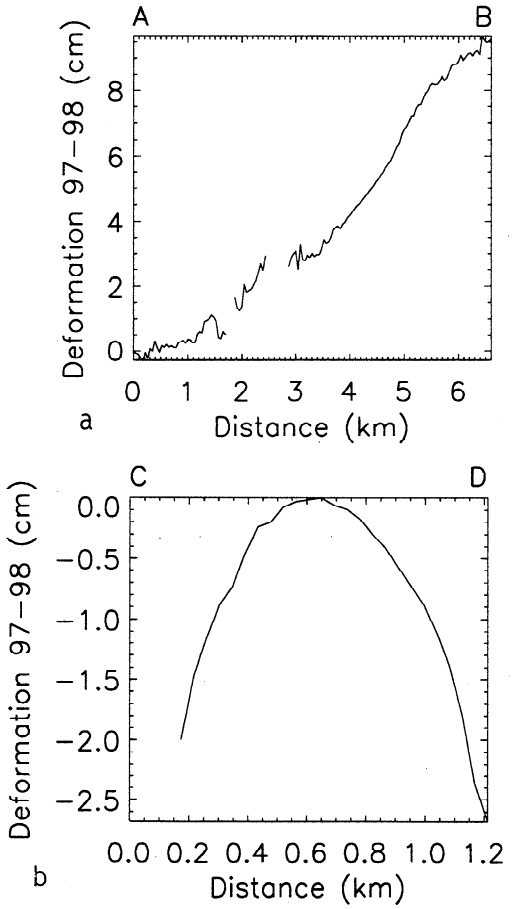

Figure 6. (a) Deformation from 1997 to 1998 along profile A-B. The positions of A and B are shown in Plate 8. (b) Deformation from 1997 to 1998 along profile C-D. The positions of C and D are shown in Plate 8.

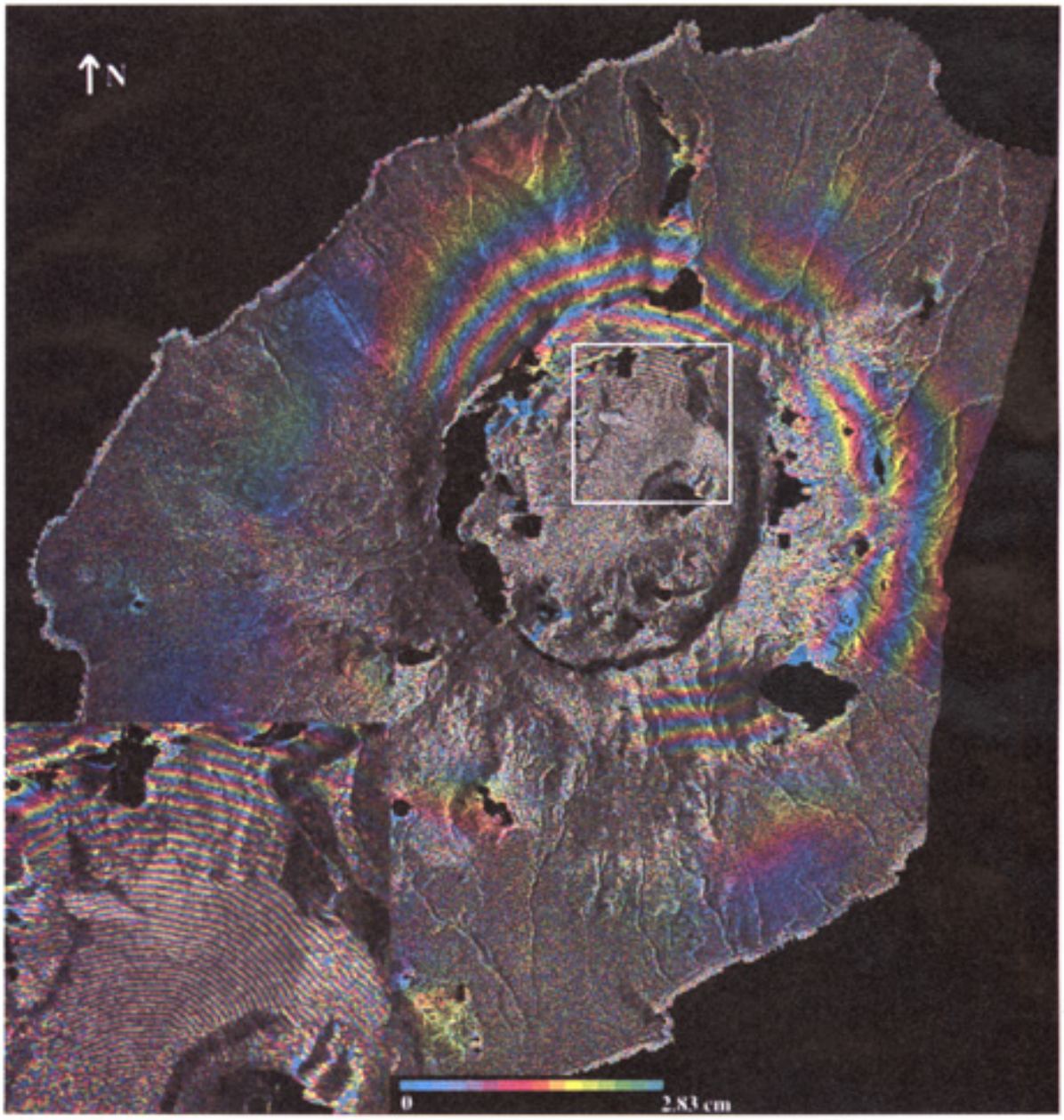

Plate 6. Deformation interferogram spanning October 9, 1995 to September 9, 1997, which brackets the February 1997 eruption of Okmok volcano. Each fringe represents a 2.83-cm deformation along the satellite look direction. A zoomed portion of the interferogram with dense fringes, outlined by the white box, is shown in the lower left corner.

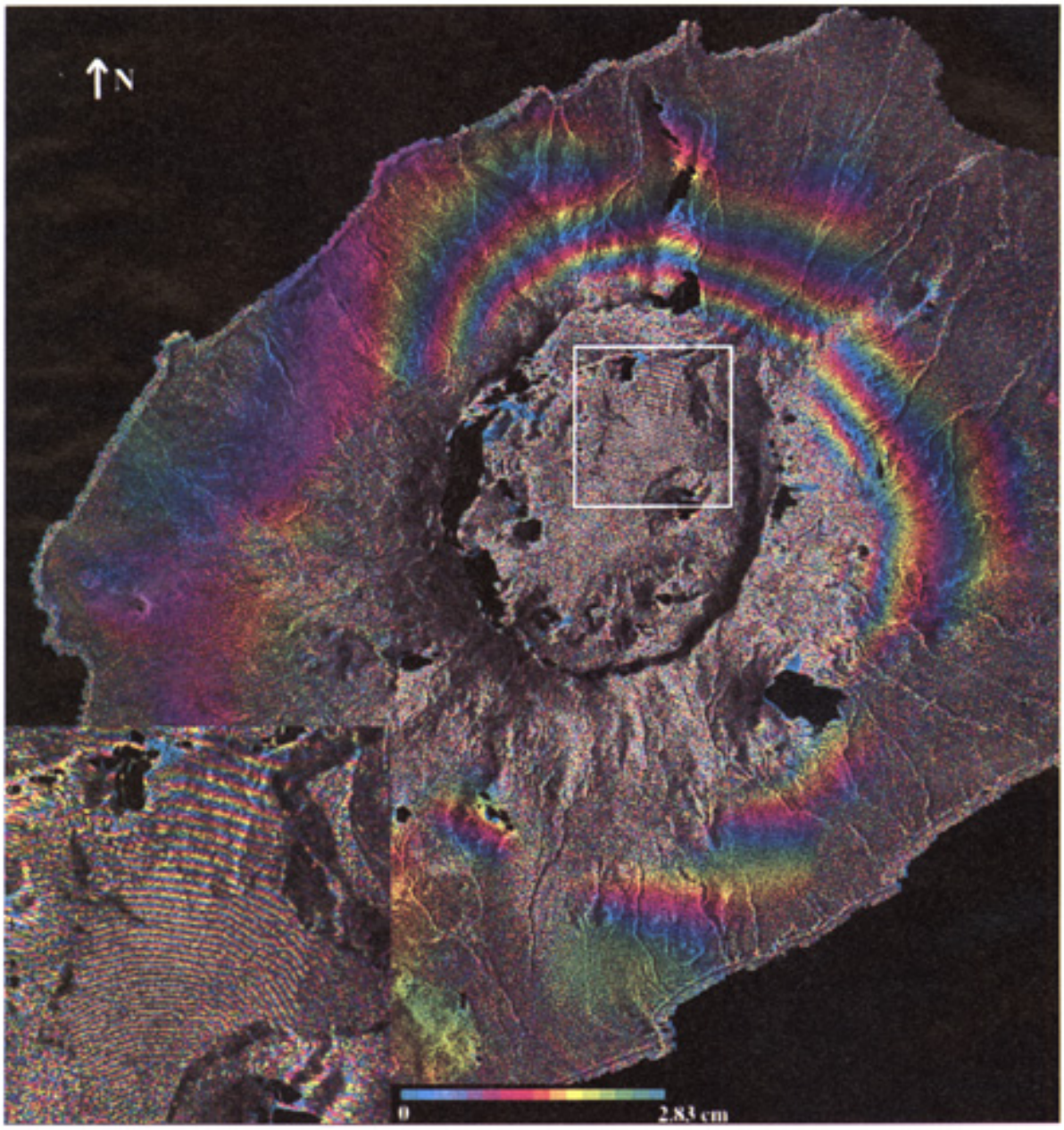

Plate 7. Deformation interferogram spanning June 7, 1995 to September 25, 1997, which brackets the February 1997 eruption of Okmok volcano. Each fringe represents a 2.83-cm deformation along the satellite look direction A zoomed portion of the interferogram with dense fringes, outlined by the white box, is shown in the lower left corner.

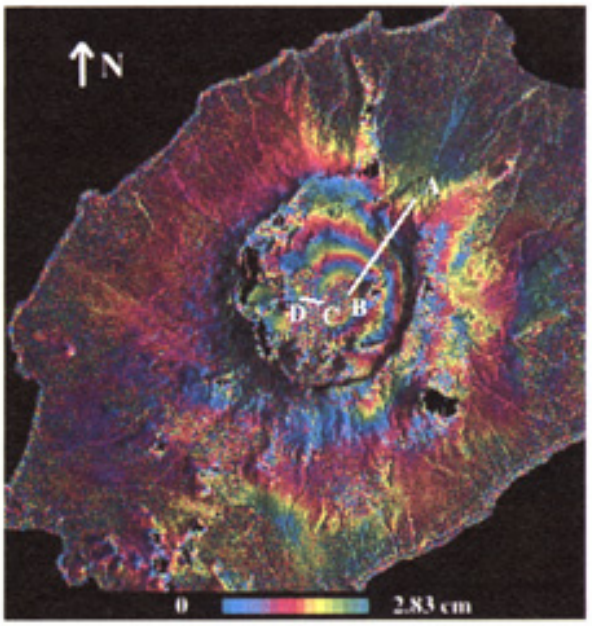

Plate 8. (a) Deformation interferogram from 1997 to 1998. Deformations along profile A-B and C-D are shown in Figures 6a and 6b, respectively. Each fringe represents a 2.83-cm deformation along the satellite look direction.

1989. They interpreted the subsidence as being caused by compaction of the recent lava flows and relaxation of the substrate in response to the loading of recently erupted materials. It will be interesting to observe the deformation of 1997 erupted lava flows using images acquired between the summers of 1998 and 1999 to see whether we can observe the subsidence effect proposed by *Briole et al.* [1997].

7. Discussion

7.1. Deformation Models and Estimation of Magma Source Parameters

We modeled the observed co-eruptive deflation (Plate 6) using a spherical point deflationary pressure source in an elastic half-space [*Mogi*, 1958]:

$$\Delta h(r) = Cd/(r^2 + d^2)^{3/2} \quad (1)$$

$$\Delta r(r) = Cr/(r^2 + d^2)^{3/2}, \quad (2)$$

where Δh and Δr are the vertical and horizontal (radial) and displacements, C is a scale factor, d is the depth of the point source, and r is the distance from the source. The scale factor C depends on the dimension of the source and the pressure change. The volume of the subsidence bowl on the surface is $2\pi|C|$. The point source approximation is valid if the size of the source dimension is much smaller than its depth. One of the drawbacks of the Mogi source is the neglect of topographic effects, which can introduce errors in deformation modeling [*Williams and Wadge*, 1998; *Cayol and Cornet*, 1998]. The caldera floor is relatively flat (~370 m), so effects of topography on the predicted surface deformation are not significant. The deflationary source in the coeruptive interferogram is inferred to be a shallow magma chamber that fully or partially emptied as a result of the 1997 eruption. We used a forward modeling approach, generating synthetic interferometric fringes for single point source deflation models with varying location, depth, and scale factor. The horizontal coordinates of the model deflation source were chosen to match the shape of the observed fringes. The source depth and scale of the pressure source were varied to match the observed fringe spacing and total number of fringes. The best fitting model has a source depth of 2.7 km. The maximum subsidence in this model is 140 cm, directly above the deflationary source. The average error of fit between the observed and modeled deformation is 1.9 cm, with maximum error of ~14.3 cm around the center of the Mogi source. A modeled interferogram with the best fitting source is shown in Plate 9, which covers the same region as Plate 6. The fringes are not circular because they indicate range changes in the direction of the satellite. The relatively small look angle for the ERS satellites (~23°) means that interferograms made from ERS images are most sensitive to vertical displacements of the ground surface. Horizontal displacements have a smaller, but nonnegligible, effect.

We can estimate the volume of lava removed from the magma chamber if certain assumptions are made. First, we must assume that the deformation resulted entirely from removal of magma and not from changes in gas pressure. Then, assuming a Poisson's ratio of 0.25, the volume change in the magma body is equal to two thirds the volume of the subsidence bowl at the surface [*Anderson*, 1936; *Sigmundsson et al.*, 1992]. Under these assumptions, with a deflationary source having a scale factor C = -0.114 km^3 (equations (1) and (2)), we inferred a volume change in the magma chamber of 0.048 km^3. This is a minimum value since we cannot know if significant inflation occurred between October 1995 and the time of the eruption. If inflation occurred, then the actual coeruptive deflation would be larger in magnitude by an amount equal to the inflation since we measure only the sum of the two. The lava covered an area of 7.5 km^2. The erupted volume probably exceeds the stored volume as a result of vesiculation, which forms bubbles in the erupted lava and increases its volume. Vesicularity of Hawaiian lava varies widely, but 15% by volume is typical (D. Dzurisin, personal communication, 1999). If we increase the stored volume by 15% to get the erupted volume, we get 0.055 km^3. This corresponds to an average lava flow thickness of 7.4 m, very close to the 8 m measured at a few spots in the field [Mann et al., 1998].

Although the areas with coherence are smaller in some of the preeruptive and posteruptive interferograms, it is clear that a point source inflation model at the same location as the deflationary source can explain those data. We find very similar locations and depths, ranging from 1.7 to 3.0 km, for the preeruptive and posteruptive interferograms. In all cases, the Mogi source is located at about the center of the caldera.

7.2. Implications of the Shallow Magma Source

The inferred magma sources for the preeruptive inflation, coeruptive deflation, and posteruptive inflation are all located at about the center of the caldera at a very shallow depth. Smaller amounts of preeruptive inflation has been observed with SAR interferometry for other volcanoes. The Radarsat interferometric observation of Piton de la Fournaise volcano [*Sigmundsson et al.*, 1999] indicated that <6 cm of inflation might have occurred 1 year before the 1998 eruption. The observation of preeruptive inflation of the Okmok caldera

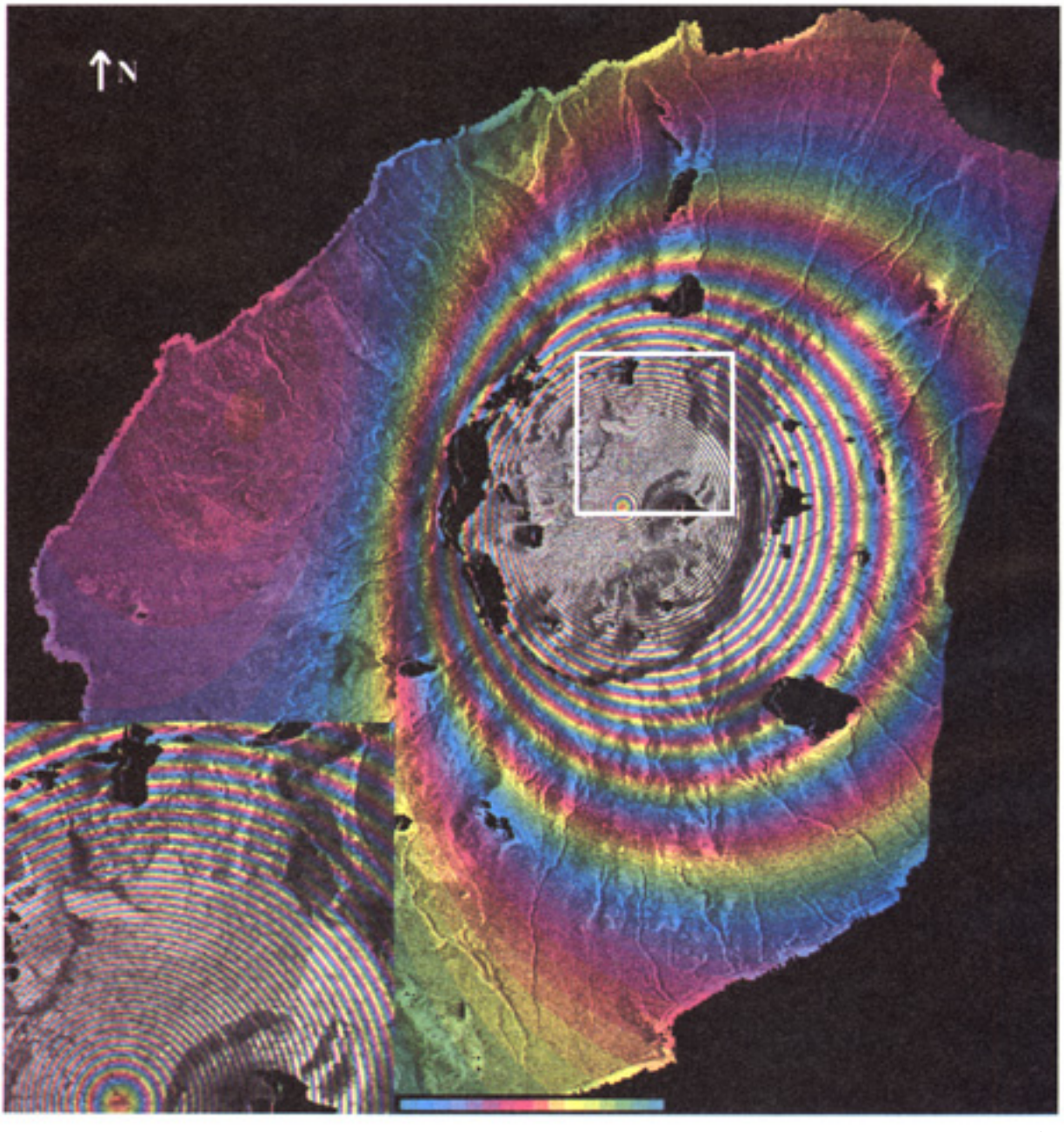

Plate 9. A modeled interferogram using the best fit point deflation model covering the same region as Plate 6. A zoomed portion of the interferogram with dense fringes, outlined by the white box, is shown in the lower left corner.

could mean that a minimum of 0.006 km^3 of magma was emplaced in a shallow magma chamber in the 3 years preceding the eruption or that pressure increased without additional magma input by development of a vapor phase.

The center of subsidence is offset by ~5 km from the eruptive vent, which implies that significant lateral magma transport might have occurred during eruption. The offset between the eruption center and the deformation center at Okmok is not unprecedented at basaltic volcanoes like Kilauea and Piton de la Fournaise. Magma accumulates in a shallow reservoir beneath the caldera, causing the ground surface to swell. Sometimes the ensuing eruption occurs in the summit area, near the center of uplift, but often magma intrudes laterally along a rift zone and the eruption site is displaced from the center of deformation. For silicic volcanoes, such as Katmai, Izu-Oshima, and Usu, eruption centers were also offset from the centers of deformation [*Newhall and Dzurisin*, 1988].

8. Conclusions

Using two-pass SAR interferometry and ERS-1 and ERS-2 images, we studied preeruptive inflation, coeruptive deflation, and posteruptive inflation for the 1997 eruption of Okmok volcano, Alaska. We also studied changes in interferometric coherence within the caldera, as well as the effect of atmospheric delays on interferometric measurement.

We observed inflation of 18 cm from 1992 to 1995 before the eruption, >140 cm of deflation associated with the eruption, and ~10 cm of inflation in the first year after the eruption. The best fitting model suggests the magma reservoir resided at a depth of 2.7 km beneath the center of the caldera, which was ~5 km from the eruptive vent. We estimated a lower bound to the volume of the erupted material to be 0.055 km^3, and the estimated average thickness of the lava flow is ~7.4 m.

By studying changes in interferometric coherence, we found that the newly erupted lava completely lost radar coherence within 3-5 months after the eruption, suggesting changes in the surface probably related to cooling and compaction. It took 5-17 months for coherence to recover. Finally, atmospheric delay anomalies for interferograms are found to be significant, and redundant observations are critical to differentiate geophysical signals from atmospheric noise.

Acknowledgments. We gratefully thank D. Dzurisin for helpful inputs regarding offset between the eruption center and the deformation center, and the vesicularity of newly erupted lava and its implication on estimating the thickness of lava flow. Constructive comments made by reviewers D. Massonnet, D. Dzurisin, and associate editor P. Delaney improved the quality of the manuscript. We thank C. Werner and H. Zebker for helpful discussion on interferometry processing, and F. H. Massmann for providing the PRC vectors. We thank the User Services at the Alaska SAR Facility (ASF) for their special efforts in making the SAR data available. USGS internal technical reviews made by T. Albright and D. Gesch are greatly appreciated. Work for this study was done at Raytheon under USGS contract 1434-CR-97-CN-40274. A NASA grant NAG5-4369 provided support to Freymueller and Mann, and partial support to Lu. The 1998 field reconnaissance of Okmok was supported by the Alaska Volcano Observatory. The ERS-1 and ERS-2 SAR images are copyright © 1992, 1993, 1995, 1997, and 1998 ESA, and provided by the ASF.

References

Anderson, E., The dynamics of the formation of cone-sheets, ring-dykes, and caldron-subsidence, *Proc. R. Soc. Edinburgh, 56*, 128-157, 1936.

Briole, P., D. Massonnet, and C. Delacourt, Post-eruptive deformation associated with the 1986-87 and 1989 lava flows of Etna detected by radar interferometry, *Geophys. Res. Lett., 24*, 37-40, 1997.

Byers, F. M., Geology of Umnak and Bogoslof Islands, Aleutian Islands, Alaska, *U.S. Geolo. Surv. Bull.*, 1028-L, 1959.

Cayol, V., and F. Cornet, Effects of topography on the interpretation of the deformation field of prominent volcanoes–Application to Etna, *Geophys. Res. Lett., 25*, 1979-1982, 1998.

Dean. K., M. Servilla, A. Roach, B. foster, and K. Engle, Satellite monitoring of remote volcanoes improves study efforts in Alaska, *Eos Trans. AGU, 79*(35), 413, 422-423, 1998.

Fujiwara, S., P. A. Rosen, M. Tobita, and M. Murakami, Crustal deformation measurements using repeat-pass JERS-1 synthetic aperture radar interferometry near the Izu Peninsula, Japan, *J. Geophys. Res., 103*, 2411-2426, 1998.

Gatelli, F., et al., The wavenumber shift in SAR interferometry, *IEEE Trans. Geosci. Remote Sens., 32*, 855-865, 1994.

Goldstein, R., H. Zebker, and C. Werner, Satellite radar interferometry: Two-dimensional phase unwrapping, *Radio Sci., 23*, 713-720, 1988.

Jonsson, S., et al., A shallow-dipping dike fed the 1995 flank eruption at Fernandina volcano, Galapagos: Observed by satellite radar interferometry, *Geophys. Res. Lett., 26*, 1077-1080, 1999.

Lanari, R., P. Lundgren, E., Sansosti, Dynamic deformation of Etna volcano observed by satellite radar interferometry, *Geophys. Res. Lett., 25*, 1541-1544, 1998.

Lu, Z., and J. Freymueller, Synthetic aperture radar interferometry coherence analysis over Katmai volcano group, Alaska, *J. Geophys. Res., 103*, 29,887-29,894, 1998.

Lu, Z., et al., Deformation of New Trident volcano measured by ERS-1 SAR interferometry, Katmai national Park, Alaska, *Geophys. Res. Lett., 24*, 695-698, 1997.

Lu, Z., D. Mann, and J. Freymueller, Satellite radar interferometry measures deformation at Okmok Volcano, *Eos Trans. AGU, 79*(39), 461, 467-468, 1998.

Mann, D., J. Freymueller, and Z. Lu, SAR interferometry as a versatile tool to investigate Okmok volcano, Alaska, *Eos Trans. AGU, 79*(45), Fall Meet. Suppl., F35, 1998.

Massmann, F. H., Information for ERS PRL/PRC users, technical note, GeoForschungsZentrum, Potsdam, Germany, 1995.

Massonnet, D., and K. Feigl, Discrimination of geophysical phenomena in satellite radar interferograms, *Geophys. Res. Lett., 22*, 1537-1540, 1995.

Massonnet, D., and K. Feigl, Radar interferometry and its application to changes in the Earth's surface, *Rev. Geophys., 36*, 441-500, 1998.

Massonnet, D., and T. Rabaute, Radar interferometry: limits and potential, *IEEE Trans. Geosci. Remote Sens., 31*, 455-464, 1993.

Massonnet, D., P. Briole, and A. Arnaud, Deflation of Mount Etna monitored by spaceborne radar interferometry, *Nature, 375*, 567-570, 1995.

Miller, T. P., et al., Historically active volcanoes of Alaska, *U.S. Geolo. Surv. Open File Rep., 98-582*, 1998.

Mogi, K., Relations between the eruptions of various volcanoes and the deformations of the ground surface around them, *Bull. Earthquake Res. Inst. Univ. Tokyo, 36*, 99-134, 1958.

Newhall, C. G., and D. Dzurisin, Historical unrest at large calderas of the world, *U.S. Geolo. Surv. Bulletin 1855*, 1108 pp., 1988.

Rosen, P., S. Hensley, H. Zebker, F. H. Webb, and E. J. Fielding, Surface deformation and coherence measurements of Kilauea volcano, Hawaii, from SIR-C radar interferometry, *J. Geophys. Res., 101*, 23109-23125, 1996.

Sigmundsson, F., P. Einarsson, and R. Bilham, Magma chamber deflation recorded by the Global Positioning System: The Hekla 1991 eruption, *Geophys. Res. Lett., 14*, 1483-1486, 1992.

Sigmundsson, F., H. Vadon, and D. Massonnet, Readjustment of the Krafla spreading segment to crustal rifting measured by satellite radar interferometry, *Geophys. Res. Lett., 24*, 1843-1846, 1997.

Sigmundsson, F., P. Durand, and D. Massonnet, Opening of an

eruptive fissure and seaward displacement at Piton de la Fournaise volcano measured by RADARSAT satellite radar interferometry, *Geophys. Res. Lett.*, *26*, 533-536, 1999.

Tarayre, H., and D. Massonnet, Atmospheric propagation heterogeneities releaved by ERS-1 interferometry, *Geophys. Res. Lett.*, *23*, 989-992, 1996.

Thatcher, W., and D. Massonnet, Crustal deformation at Long Valley Caldera, eastern California, 1992-1996, inferred from satellite radar interferometry, *Geophys. Res. Lett.*, *24*, 2519-2522, 1997.

U.S. Geological Survey (USGS), Digital elevation models: Data users guide, Reston, Vi., 1993.

Wicks, C., W. Thatcher, and D. Dzurisin, Migration of fluids beneath Yellowstone Caldera inferred from satellite radar interferometry, *Science*, *282*, 458-462, 1998.

Williams, C.A., and G. Wadge, The effects of topography on magma chamber deformation models: Application to Mt. Etna and radar interferometry, *Geophys. Res. Lett.*, *25*, 1549-1552, 1998.

Worley, S., P. Izbekov, K. Dean, and J. Dehr, Analysis of a lava flow using satellite imagery: 1997 eruption of Okmok volcano, Alaska, *Eos Trans. AGU*, *79*(45), Fall Meet. Suppl., F957, 1998.

Wu, X., K. Thiel, and A. Wehr, The effects of different land covers on the accuracy of interferometric DEM, paper presented at FRINGE 96 ESA Workshop on Applications of ERS SAR Interferometry, Eur. Space Agency, Zurich, 1996.

Zebker, H., and J. Villasenor, Decorrelation in interferometric radar echoes, *IEEE Trans. Geosci. Remote Sens.*, *30*, 950-959, 1992.

Zebker, H., C. Werner, P. Rosen, and S. Hensley, Accuracy of topographic maps derived from ERS-1 interferometric radar, *IEEE Trans. Geosci. Remote Sens.*, *32*, 823-836, 1994a.

Zebker, H., P. Rosen, R. Goldstein, A. Gabriel, and C. Werner, On the derivation of coseismic displacement fields using differential radar interferometry: The Landers earthquake, *J. Geophys. Res.*, *99*, 19,617-19,634, 1994b.

Zebker, H., et al., Analysis of active lava flows on Kilauea volcano, Hawaii, using SIR-C radar correlation measurements, *Geology*, *24*, 495-498, 1996.

Zebker, H., P. Rosen, and S. Hensley, Atmospheric effects in interferometric synthetic aperture radar surface deformation and topographic maps, *J. Geophys. Res.*, *102*, 7547-7563, 1997.

J. T. Freymueller and D. Mann, Geophysical Institute, University of Alaska, Fairbanks, AK 99775. (jeff@giseis.alaska.edu; doerte@giseis.alaska.edu)

Z. Lu and D. Meyer, Raytheon STX Corporation, EROS Data Center, U.S. Geological Survey, Sioux Falls, SD 57198. (lu@edcmail.cr.usgs.gov; dmeyer@edcmail.cr.usgs.gov)

(Received June 7, 1999; revised November 23, 1999; accepted January 27, 2000.)